Effects of circulation on tropical cloud feedbacks in high-resolution simulations

Anna Mackie[1] and Michael Byrne[2]

[1]University of St Andrews
[2]University of St Andrews,University of Oxford,University of St Andrews

November 22, 2022

Abstract

Uncertainty in the response of clouds to global warming remains a significant barrier to reducing uncertainty in climate sensitivity. A key question is the extent to which the dynamic component – that which is due to changes in circulation rather than changes in the thermodynamic properties of clouds – contributes to the total cloud feedback. Here, simulations with a range of cloud-resolving models are used to quantify the impact of circulation changes on tropical cloud feedbacks. The dynamic component of the cloud feedback is substantial for some models and is controlled both by SST-induced changes in circulation and nonlinearity in the climatological relationship between clouds and circulation. Differences in the longwave and shortwave dynamic components across models are linked to the extent to which ascending regions narrow or expand in response to a change in SST. The diversity of changes in ascent area is coupled to intermodel differences non-radiative diabatic heating in ascending regions.

Effects of circulation on tropical cloud feedbacks in high-resolution simulations

Anna Mackie[1], Michael P. Byrne[1,2]

[1]School of Earth and Environmental Sciences, University of St Andrews
[2]Atmospheric, Oceanic and Planetary Physics, University of Oxford

Key Points:

- Influence of circulation changes on cloud feedbacks is substantial in some cloud resolving models
- Component of cloud feedback associated with circulation changes is coupled to ascent area
- Intermodel spread in response of ascent area linked to non-radiative diabatic heating

Corresponding author: Anna Mackie, arm33@st-andrews.ac.uk

Abstract

Uncertainty in the response of clouds to global warming remains a significant barrier to reducing uncertainty in climate sensitivity. A key question is the extent to which the dynamic component – that which is due to changes in circulation rather than changes in the thermodynamic properties of clouds – contributes to the total cloud feedback. Here, simulations with a range of cloud-resolving models are used to quantify the impact of circulation changes on tropical cloud feedbacks. The dynamic component of the cloud feedback is substantial for some models and is controlled both by SST-induced changes in circulation and nonlinearity in the climatological relationship between clouds and circulation. Differences in the longwave and shortwave dynamic components across models are linked to the extent to which ascending regions narrow or expand in response to a change in SST. The diversity of changes in ascent area is coupled to intermodel differences non-radiative diabatic heating in ascending regions.

Plain Language Summary

Clouds influence Earth's energy balance by absorbing and reflecting solar and terrestrial radiation. The response of clouds to warming remains a key source of uncertainty in our understanding on how the climate system will evolve. In particular, how the influence of clouds on radiation is coupled to the atmospheric circulation is an open question. In this study, idealized simulations of the tropics at high resolution (3 km) are analyzed to probe how changes in circulation impact clouds in a warming climate. It is found that, across a range of models, the degree to which circulation changes influence clouds depends on how the area of the region with ascending air responds to warming.

1 Introduction

The interplay between clouds and the atmospheric circulation is a persistent source of uncertainty in our understanding of how the climate system may evolve (Sherwood et al., 2014; Bony et al., 2015; Ceppi et al., 2017; Webb et al., 2017). One particular challenge is that clouds and their associated radiative effects – particularly in the tropics – are strongly influenced by convection (Hartmann et al., 2001), which occurs at horizontal scales smaller than those typically resolved by the current generation of global climate models (GCMs). Integrating GCMs at convection-permitting resolutions for long enough to study climate and climate change remains prohibitively expensive. One way to overcome this computational barrier is through the use of limited-domain cloud-resolving models (CRMs), which have the potential to advance fundamental understanding of cloud–circulation coupling in the tropics and shed light on potential sources of uncertainty in cloud feedbacks.

Cloud radiative effect – defined as the difference between all-sky and clear-sky broadband fluxes at the top-of-atmosphere (TOA), with positive values representing a net downward flux at TOA due to clouds – is tightly coupled to the atmospheric circulation (Bony et al., 2004). In the tropics, regions of strong ascent (Fig. 1, left column) are associated with strong positive longwave cloud radiative effects due to their high, cold cloud tops and therefore large temperature contrast relative to the surface (Fig. 1, middle column). These deep convective clouds are also highly reflective, resulting in co-located regions of strong negative shortwave cloud radiative effect (Kiehl, 1994; Hartmann et al., 2001) (Fig. 1, right column).

There are number of ways in which tropical convective-scale circulations may change in a warming climate, and it remains unclear to what extent these changes could impact cloud feedbacks. For example, previous work with CRMs has suggested that a warmer climate may lead to stronger updraft velocities (Singh & O'Gorman, 2015); more convective available potential energy (Romps & Kuang, 2011); changes to convective organization (Wing & Emanuel, 2014); a weakening of the overturning circulation and changes to the area of ascending air (Cronin & Wing, 2017; Jenney et al., 2020).

The dependence of clouds on circulation is often characterized by discretizing cloud radiative effect as a function of circulation regime, typically defined as the mid-tropospheric vertical velocity (Bony et al., 2004, 2006; Wyant, Bretherton, et al., 2006; Byrne & Schneider, 2018; Lutsko, 2018) (Fig. 2a,b). Previous work has shown that there exists an approximately linear relationship between cloud radiative effect and vertical velocity in GCMs with $\mathcal{O}(1^\circ)$ horizontal resolution for a broad range of circulation regimes (Byrne & Schneider, 2018), and that this quasi-linearity constrains the influence of circulation changes on cloud feedbacks to be small (Wyant, Bretherton, et al., 2006; Byrne & Schneider, 2018). But as $\mathcal{O}(1^\circ)$-resolution GCMs cannot resolve the convective-scale circulations that influence cloud radiative effect, particularly in tropical and subtropical regions, this begs the question: Is the impact of circulation changes on cloud feedbacks small when convection is explicitly simulated? Or do circulation changes and their impacts on cloud feedbacks become more dominant at higher resolutions, representing a potentially important influence on clouds feedbacks that is absent from the current generation of GCMs?

This study will address the following questions: First, do the climatological relationships between circulation and cloud radiative effect in CRMs have the same quasi-linearity as noted in GCMs? Second, in CRMs, is the dynamic component of cloud feedback – due to changes in circulation – a significant part of the total feedback? And third, which physical processes control the dynamic component of the cloud feedback across a range of CRMs? We begin with an overview of the models and simulations to be analyzed (Section 2), followed by a description of how cloud feedbacks are decomposed into dynamic and thermodynamic components (Section 3). We then develop, in Section 3.1, a toy model to explore the effects of nonlinearities in climatological cloud-circulation cou-

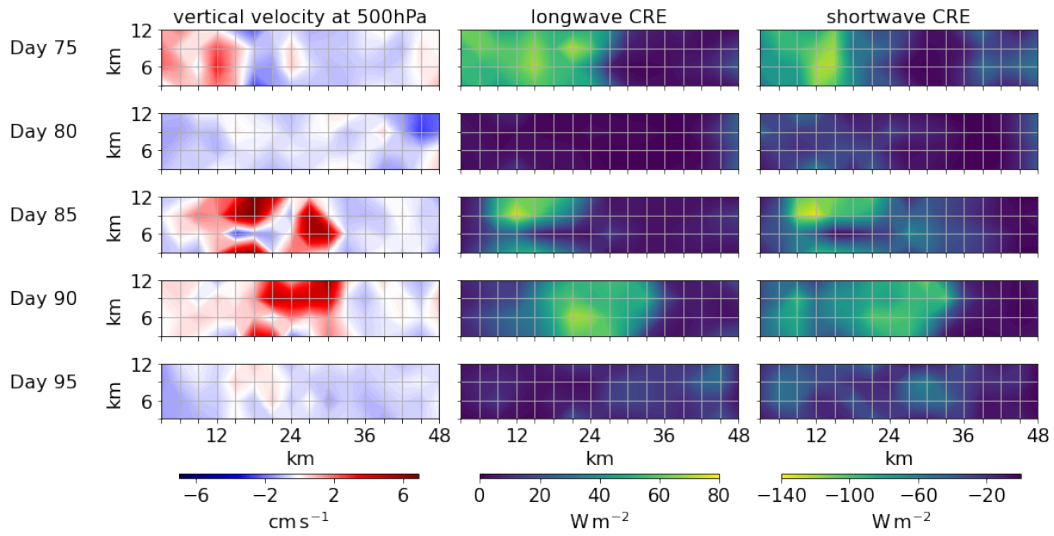

Figure 1. Daily mean snapshots of vertical velocity at 500hPa (left), longwave cloud radiative effect (LW CRE, middle) and shortwave cloud radiative effect (SW CRE, right) from the SAM_CRM RCE_large300 experiment. Data have been spatially (96 km^2 blocks) and temporally averaged (24-hour periods). Positive values of cloud radiative effect correspond to a warming effect of clouds at TOA.

pling on cloud feedbacks. In Sections 4 and 5 we analyze the physical processes controlling the dynamic components of the cloud feedback across CRMs. We conclude with a discussion and suggestions for future research (Section 6).

2 Simulations

A common framework to study cloud-circulation interactions is radiative-convective equilibrium (RCE), an idealization of the tropical atmosphere defined by a simple thermodynamic balance between radiative cooling and convective warming of the atmosphere (e.g. Held et al., 1993). A major advantage of RCE is there are no external forcings or boundary conditions from large-scale dynamics, allowing fundamental convective and cloud processes to be studied without additional complications (Wing et al., 2020). RCE can be implemented across spatial scales and for studying many different aspects of the tropical atmosphere: For example, previous studies have focused on factors controlling cloud anvil amount in GCMs and CRMs (Bony et al., 2016); the relationship between the organization of convection and extreme precipitation (Pendergrass et al., 2016; Bao et al., 2017); energetic constraints on large-scale circulation (Jenney et al., 2020); the response of updraft velocities to warming (Singh & O'Gorman, 2015); and self aggregation of convection (Bretherton et al., 2005; Muller & Held, 2012; Wing & Emanuel, 2014; Holloway & Woolnough, 2016). In this study we will primarily use CRMs to assess the degree to which circulation influences cloud feedbacks in simulations of RCE.

One area of recent focus has been convective self aggregation - the phenomenon of convection spontaneously organising in the absence of external forcing - and the interactions between the moist-radiative processes associated with it (e.g. Bretherton et al., 2005; Wing & Emanuel, 2014; Wing & Cronin, 2016a; Holloway & Woolnough, 2016; Cronin & Wing, 2017; Becker & Wing, 2020). In particular, there has been much interest in the implications of convective aggregation for equilibrium climate sensitivity (ECS). Defined as the change in global mean surface temperature at equilibrium in response to a sudden doubling of CO_2, ECS remains stubbornly uncertain in current GCMs (Zelinka et al., 2020; Sherwood et al., 2020), leading to interest in the links between climate sensitivity and aggregation in more idealized model configurations (e.g. Wyant, Khairoutdinov, & Bretherton, 2006; Cronin & Wing, 2017; Coppin & Bony, 2018; Romps, 2020). Self-aggregation is sensitive to domain size, resolution and SST (e.g Muller & Held, 2012; Wing et al., 2017; Wing, 2019), but comprehensive assessments of the phenomenon have been hampered by a lack of consistent experiments across models.

To address this, a recent model intercomparison project (the Radiative-Convective Equilibrium Intercomparison Project, RCEMIP) has established an archive of CRM and GCM simulations over a range of resolutions and SSTs (Wing et al., 2018, 2020). Despite uniform boundary conditions, there are substantial differences in RCE state across the RCEMIP simulations, with large differences in temperature, relative humidity and cloud profiles (Wing et al., 2020). Cloud and circulation responses to warming also vary across models (Becker & Wing, 2020; Silvers et al., submitted), though the majority of models simulate anvil clouds which rise, warm and reduce in area fraction with SST warming, consistent with previous work (Hartmann & Larson, 2002; Zelinka & Hartmann, 2010; Bony et al., 2016).

The RCEMIP models also have a large spread in their "Cess-type" TOA feedback parameters (Cess & Potter, 1988) – defined as the change in net TOA radiation divided by the surface temperature change – leading to a spread in their hypothetical climate sensitivities (Wing et al., 2020; Becker & Wing, 2020). Becker and Wing (2020) determine that model differences in the total feedback parameter and climate sensitivity arise through a combination of shallow cloud fraction and convective aggregation, but that it is changes in the degree of self aggregation which influences the feedback parameter rather than the average value.

A major advantage of RCEMIP is that it incorporates a hierarchy of models run in RCE, with consistent experiments allowing comparison across model types. Here, we focus on the simulations at cloud resolving (3 km) resolution in a long-channel domain ($\sim$ 6000 km x $\sim$ 400 km). These long-channel simulations permit both convection and the evolution of large-scale dynamics within the domain (Wing & Cronin, 2016b; Cronin & Wing, 2017). We use all the CRM long-channel simulations which provide the variables required for our analysis. All models used are listed in Table Appendix A. Detailed information about individual models can be found in the supporting information of Wing et al. (2020). All simulations are non rotating, with uniform solar insolation and uniform, fixed SST at three different temperatures (295, 300 and 305 K). We exclude two models from all our analysis (UCLA-CRM and MESONH) at the higher temperature range (305-300 K) because their simulations are highly anomalous and have an undue effect on our analysis (Fig. S1).

3 Dynamic and thermodynamic components of cloud feedbacks

To assess how circulation changes influence cloud feedbacks we follow the framework introduced by Bony et al. (2004), and employed by a number of subsequent studies (Wyant, Bretherton, et al., 2006; Wyant, Khairoutdinov, & Bretherton, 2006; Byrne & Schneider, 2018; Lutsko, 2018), in which changes in the cloud radiative effect at TOA are decomposed into components associated with a) changes in circulation (the dynamic component) and b) changes assuming fixed circulation (the thermodynamic component). The nonlinear component quantifies the combined influence of changes in circulation and thermodynamic processes.

We analyze the last 25 days of each simulation, following Wing et al. (2020). For the CRMs, we perform spatial and temporal averaging: We calculate daily means with a spatial average over 96 km^2, a similar scale to typical GCM gridboxes which have a resolution on the order of 1-2°.

To decompose the total cloud feedback in dynamic and thermodynamic components, we first characterise how the cloud radiative effect, in both the longwave and shortwave, depends on vertical velocity at 500 hPa (w). We extract the vertical velocity at the model level closest to 500 hPa for each time- and space-averaged block, then discretize the vertical velocity field into bins of width 0.001 ms^{-1}. This allows us to construct two discretized functions of the longwave and shortwave cloud radiative effects, $R_{LW}(w)$ and $R_{SW}(w)$, which we term the "cloud-circulation coupling functions". Figures 1 and 2 illustrate this process: for all the grid points falling within a particular vertical velocity bin (Fig. 1, left column), we calculate the mean of the longwave and shortwave cloud radiative effects (Fig. 1, middle and right columns) obtaining $R_{LW}(w)$ and $R_{SW}(w)$ (Fig. 2 a,b). The area probability density function $[A(w)]$ is simply the normalized number of points within each vertical velocity bin (Fig. 2c). To construct a continuous function, we linearly interpolate across any empty vertical velocity bins and ensure $A(w)$ integrates to 1 over the full w range by applying a correction to account for the linear interpolation.

Figure 2a-c shows the $R_{LW}(w)$, $R_{SW}(w)$ and $A(w)$ functions from the SAM_CRM model in turquoise. Also included are the multimodel mean, interquartile range and full range of the CRMs. Despite the large intermodel spread, there are some common features across models: While there are relatively few grid points with strong ascent (strongly positive vertical velocity), these regions have large longwave and shortwave cloud radiative effects associated with deep convective clouds. These high-topped clouds are both cold, reducing the outgoing longwave radiation with respect to clear-sky conditions and producing a strong positive longwave cloud radiative effect, and reflective, increasing the proportion of shortwave radiation reflected to space and producing a strong negative shortwave cloud radiative effect. With weakening ascent, we generally see a decrease in the magnitudes of the longwave and shortwave cloud radiative effects (Fig. 2a,b).

Written in continuous form, the mean change in cloud radiative effect with warming, $\overline{\delta R}$, is decomposed into dynamic, thermodynamic and nonlinear components as follows:

$$\overline{\delta R} = \underbrace{\int_{-\infty}^{\infty} R(w)\delta A(w)\mathrm{d}w}_{\text{dynamic}} + \underbrace{\int_{-\infty}^{\infty} \delta R(w)A(w)\mathrm{d}w}_{\text{thermodynamic}} + \underbrace{\int_{-\infty}^{\infty} \delta R(w)\delta A(w)\mathrm{d}w}_{\text{nonlinear}}\,. \tag{1}$$

The first term on the right hand side of (1) is the dynamic component representing the effect of circulation changes between simulations, $\delta A(w)$, on cloud radiative effect assuming constant cloud–circulation coupling functions (i.e. $\delta R_{LW}(w) = 0$, $\delta R_{SW}(w) = 0$). The second term is the thermodynamic component, which quantifies the change in cloud radiative effect assuming a fixed distribution of vertical velocity (i.e. $\delta A(w) = 0$). The third term is the nonlinear component, which depends on changes in both circulation and cloud–circulation coupling. In physical terms, the dynamic component represents the change in cloud radiative effect due to, say, a strengthening or weakening of vertical velocity in ascending/descending regions, or a change in the relative sizes of these regions, while the thermodynamic component includes, for example, the effects on the cloud radiative effect of phase changes in cloud water. For discussion of these and further examples we refer the reader to Byrne and Schneider (2018).

3.1 Influence of nonlinearity in cloud–circulation coupling on the dynamic component

As illustrated in Figure 2, the cloud–circulation coupling functions $R_{LW}(w)$ and $R_{SW}(w)$ are approximately linear over a range of vertical velocities, a feature also found in observations and reanalyses (Bony et al., 2004; Wyant, Bretherton, et al., 2006) and global

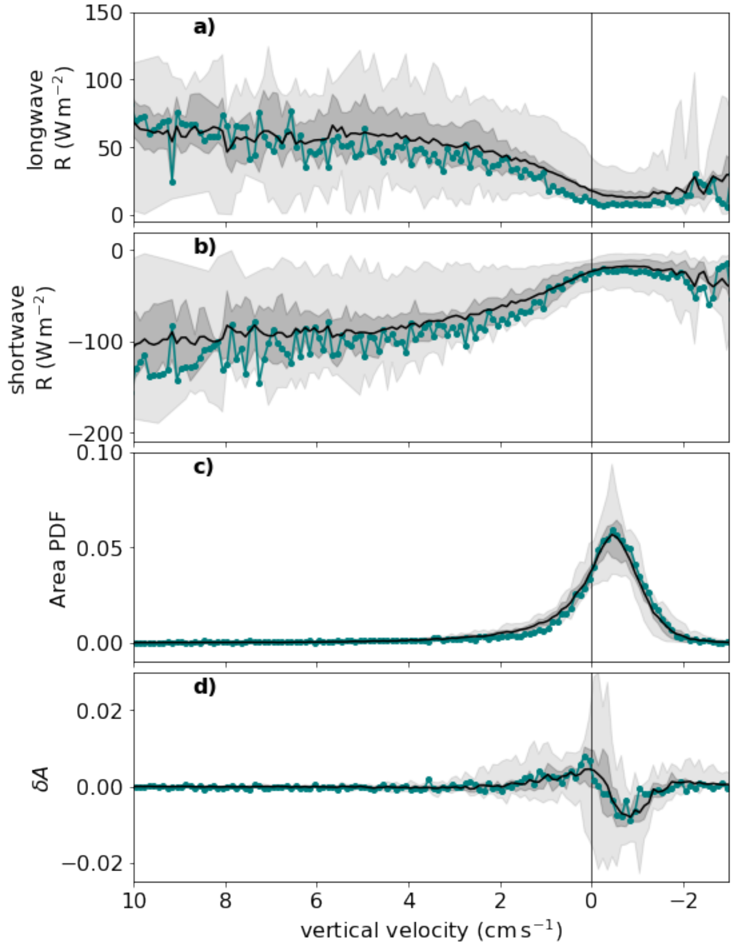

Figure 2. (a) Longwave cloud radiative effect, (b) shortwave cloud radiative effect and (c) area probability density function (PDF) expressed as functions of vertical velocity at 500 hPa for the 300 K simulations. (d) Change in area PDFs between the 300 K and 305 K simulations. Light grey shading indicates the full range of RCEMIP models, dark grey shading the interquartile range, and the black continuous lines show the multimodel means. Data from SAM_CRM is in turquoise.

coupled models (Byrne & Schneider, 2018). This quasi-linearity constrains the global dynamic component of the cloud feedback to be small in GCMs (Byrne & Schneider, 2018); we summarize this argument below before exploring, using a toy model, how different characteristics of the nonlinearity in cloud–circulation coupling control the degree to which circulation changes influence the cloud feedback.

The dynamic component of the cloud feedback is defined as [see (1)]:

$$\overline{\delta R}_{dyn} = \int_{-\infty}^{\infty} R(w)\delta A(w)\mathrm{d}w. \tag{2}$$

Substituting a linearized form of the cloud–circulation coupling function, $R_{lin}(w) = a + bw$ where a and b are constants, into (2), the dynamic component can be expressed as a sum of two terms (Byrne & Schneider, 2018): $\overline{\delta R}_{dyn}^{lin} = a\int_{-\infty}^{\infty}\delta A\mathrm{d}w + b\int_{-\infty}^{\infty} w\delta A\mathrm{d}w$. The first term on the right hand side of this expression is zero because $A(w)$ is a normalized area PDF, implying by definition that any change in $A(w)$ integrates over w to zero. The second term is also zero by mass conservation: For any given climate state – and averaged over a sufficiently long time and over a region with zero net mass flux across its boundary (i.e. a closed-mass region) – the total mass flux of the ascending region (where $w > 0$) balances the total mass flux of the descending region (where $w < 0$) such that $\int_{-\infty}^{0} wA\mathrm{d}w = -\int_{0}^{\infty} wA\mathrm{d}w$ and $\int_{-\infty}^{\infty} wA\mathrm{d}w = 0$.

The argument above demonstrates that if the relationship between vertical velocity and cloud radiative effect is strictly linear, circulation changes are irrelevant for cloud feedbacks when averaged over a sufficiently large region (Wyant, Bretherton, et al., 2006; Byrne & Schneider, 2018). But in the more general case where cloud–circulation coupling functions are nonlinear, the dynamic component will depend on higher-order terms in w that do not generally integrate to zero when multiplied by $\delta A(w)$.

We extend this theoretical analysis to demonstrate that not only is a nonlinear cloud–circulation coupling function required for a nonzero dynamic component, but that the magnitude of the dynamic component depends on both the degree of nonlinearity in $R(w)$ and its location, in w space, relative to the change in circulation, $\delta A(w)$. To illustrate the sensitivities of the dynamic component to the climatological structure of cloud–circulation coupling, we construct a toy model of $R(w)$:

$$R_{toy}(w) = a + bw + c\tanh(dw + e), \tag{3}$$

where a, b, c, d and e are constants, with baseline values of $a = 17$, $b = 592$, $c = 32$, $d = 1$ and $e = 0$. The functional form of (3) and values of the constants are chosen so as to qualitatively match a simulated longwave cloud–circulation coupling function (cf. Fig. 3a and Fig. 3b). By varying the constants c and e we explore, respectively, the impacts on the dynamic component of (i) varying the degree of nonlinearity in $R(w)$ and (ii) varying the location of the nonlinearity relative to $\delta A(w)$ in w space. The stylized version of $R(w)$ described by (3) is multiplied by the simulated circulation change $\delta A(w)$ from the SAM_CRM model and summed over all vertical velocities to explore, in a general way, how climatological cloud–circulation coupling affects the cloud feedback.

As anticipated from the discussion above and following the results of Byrne and Schneider (2018), when $R(w)$ is linear ($c = 0$, turquoise line in Fig. 3b), the resultant dynamic component is identically zero (turquoise circle in Fig. 3d). As the nonlinearity is enhanced by increasing c, the magnitude of the dynamic component increases (Fig. 3d). As a more intuitive measure of the nonlinearity, we plot the the dynamic component against 'step size', defined as the difference, in Wm^{-2}, between the two linear extrapolations before and after the nonlinearity. These extrapolations are shown in Fig. 3b for the case of $c = 48$ as dashed red lines. Thus, Fig. 3d shows that the magnitude of the dynamic effect increases approximately linearly with step size.

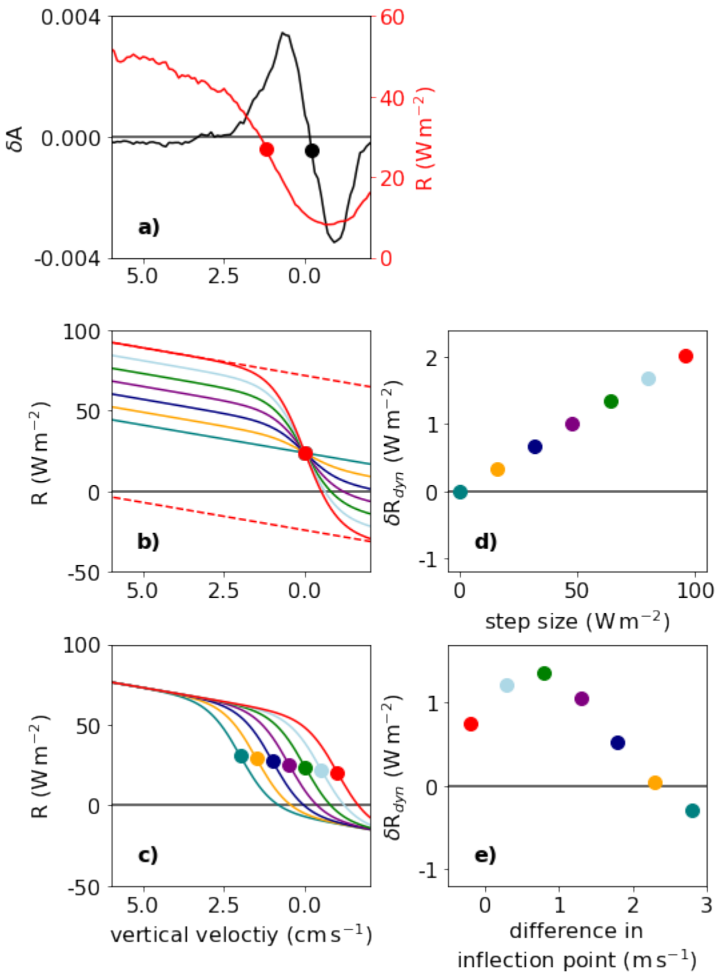

Figure 3. Investigating the effects of nonlinearity in cloud–circulation coupling using a toy model of $R(w)$. (a) Simulated $R(w)$ taken from the SAM_CRM RCE_large300 run, while δA is calculated from SAM_CRM RCE_large305 minus SAM_CRM RCE_large300. Both $R(w)$ and δA are smoothed using a 14-bin moving average over w. Idealized forms of $R(w)$ generated using (3) by varying the (b) step size and (c) point of inflection. Circles in plots (a)-(c) indicate location of the inflection point in the function. (d) and (e): The dynamic components obtained by multiplying the idealized forms of $R(w)$ from (b) and (c), respectively, with the simulated δA from (a), as a function of (d) step size and (e) the difference in inflection points between $\delta A(w)$ and $R(w)$, and integrating over w.

Varying the location of the nonlinearity in the cloud–circulation coupling function with respect to $\delta A(w)$ (Fig. 3c) also impacts the dynamic component (Fig. 3e). In particular, we plot the dynamic component as a function of the 'difference in inflection points' (Fig. 3c), which is varied using the e parameter in (3). The difference in inflection points is defined, in units of ms^{-1}, as the position of the inflection point in $R(w)$ minus the position of the inflection point in $\delta A(w)$ (see circles in Fig. 3a). Figure 3e demonstrates that the magnitude of the dynamic component varies non-monotonically with the difference in inflection point and can be either a positive (warming) or negative (cooling) feedback depending on the structure of cloud–circulation coupling relative to the structure of the circulation change.

Using this toy model, we show that not only does a nonzero dynamic component require the climatological cloud–circulation coupling function to be nonlinear, but the size of the nonlinearity and its location in vertical velocity space influence the magnitude of the dynamic component. Therefore the characteristics of climatological cloud–circulation coupling are crucial for determining how changes in circulation affect cloud feedbacks.

4 Dynamic component across cloud-resolving models

The remainder of this paper focuses on the dynamic component of cloud feedbacks across the RCEMIP CRMs. We begin by quantifying the role of circulation changes in cloud feedbacks before assessing whether intermodel spread in the dynamic component is controlled primarily by differences in circulation changes or differences in climatological cloud–circulation coupling across models (Section 4.1). This is followed by an investigation of how the dynamic component depends on bulk metrics of the atmospheric circulation (Section 4.2), with a focus on the physical processes controlling ascent fraction (Section 5).

4.1 Quantifying the dynamic component of the cloud feedback

Using the decomposition (1), we calculate the total cloud feedback as well as the dynamic, thermodynamic and nonlinear components for both temperature differences (300 minus 295 K and 305 minus 300 K), and for the models listed in Table Appendix A. We verify that the sum of the feedback components [see (1)] is approximately equal to the total cloud feedback calculated by taking the change in domain-mean cloud radiative effects between two simulations with different SSTs and dividing by the SST change. The multi-model mean difference between the two methods is $\sim 0.01\ \mathrm{Wm^{-2}K^{-1}}$ for both the longwave and shortwave feedbacks.

The longwave thermodynamic component across models ranges from approximately -1 to +1 $\mathrm{Wm^{-2}K^{-1}}$, which is a larger range than the dynamic component (approximately -0.5 to 0.5 $\mathrm{Wm^{-2}K^{-1}}$). However, both the thermodynamic and dynamic components have a statistically significant ($p < 0.01$) correlation with the total cloud feedback (e.g. $r^2 = 0.94$, 0.65 for the longwave thermodynamic and dynamic components, respectively). The correlation between the total shortwave feedback and the dynamic component is less strong ($r^2 = 0.18$) and not statistically significant. A statistically significant correlation between the dynamic and thermodynamic components in the longwave ($r^2 = 0.43$) suggests that the processes determining the magnitude of the two components are not independent, though this does not apply in the shortwave ($r^2 = 0.00$ for the correlation between the thermodynamic and dynamic components).

In summary, the longwave and shortwave dynamic components are (i) substantial in magnitude compared to the total feedbacks; and (ii) linked to differences in total cloud feedback across models, at least in the longwave. An immediate question arising from this analysis is whether intermodel differences in the dynamic component are primarily due to differences in climatological cloud–circulation coupling [i.e. different $R(w)$ func-

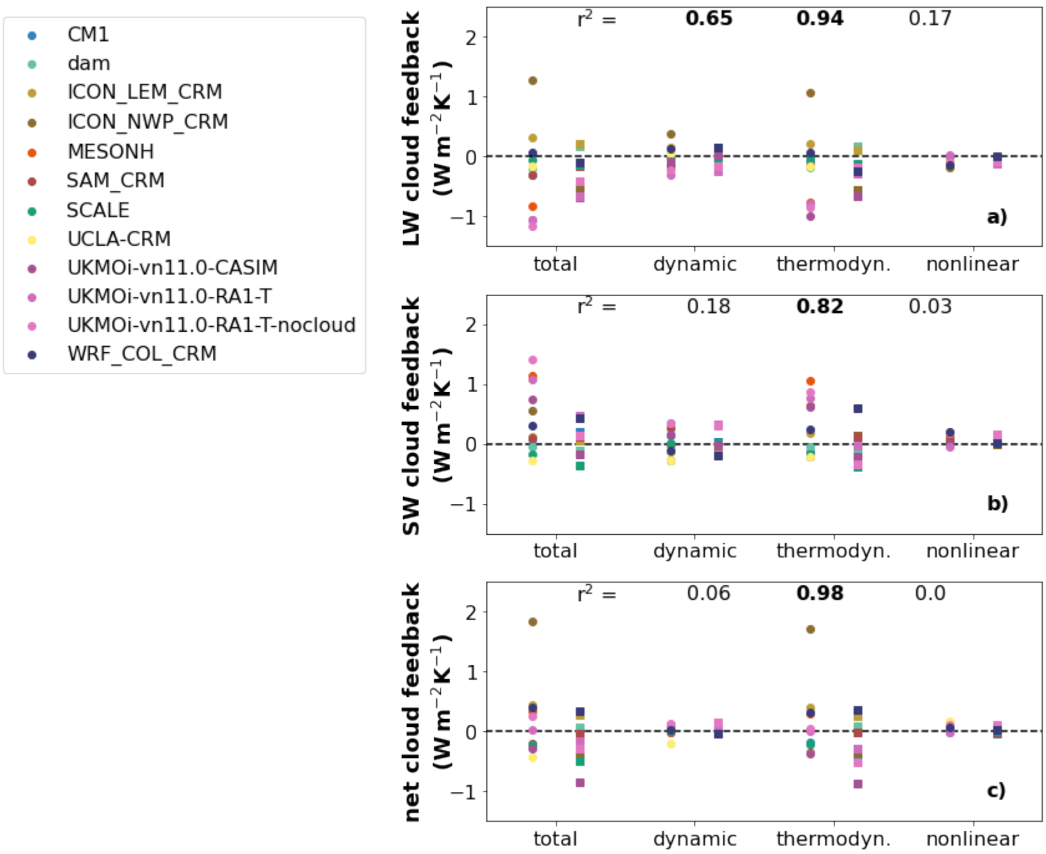

Figure 4. Total (a) longwave, (b) shortwave and (c) net cloud feedbacks, along with the dynamic, thermodynamic and nonlinear components as defined by (1), for the RCEMIP CRMs. Feedbacks computed between the 295 K and 300 K simulations (circles) and the 300 K and 305 K simulations (squares) are shown. Numbers at the top of each subplot indicate the Pearson correlation coefficient between the total cloud feedback and the various feedback components, across all models and both temperature changes. The correlations written in bold are statistically significant ($p < 0.01$). Feedbacks for the UCLA-CRM and MESONH models computed using the 300 K and 305 K simulations have been omitted as they are significant outliers (see Section 4.1 and Fig. S1).

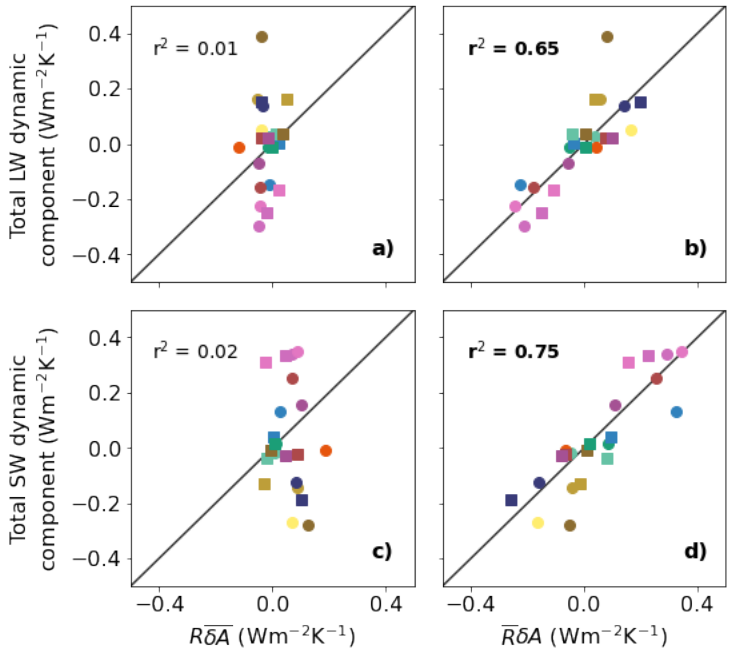

Figure 5. (a) Longwave and (c) shortwave dynamic components calculated using the multimodel-mean change in circulation $[\overline{\delta A(w)}]$ and model-specific cloud–circulation coupling functions $[R(w)]$, plotted against the full dynamic component calculated using (1). (b,d) As in panels (a) and (c) but here, for the x-axis, computing the longwave and shortwave dynamic components using the multimodel-mean cloud–circulation coupling function $[\overline{R(w)}]$ and the model-specific circulation changes $[\delta A(w)]$. Colours represent different models, corresponding to the legend in Figure 4. Dynamic component is calculated using the 295 K and 300 K simulations (circles) and the 300 K and 305 K simulations (squares). Numbers at the top of each subplot indicate the Pearson correlation coefficient between the x and y axes.

tions], or differences in circulation changes with warming [i.e. different $\delta A(w)$]. To explore this question, we determine to what extent variations in the dynamic component across models can be reproduced using either the multimodel-mean cloud–circulation coupling function, $\overline{R(w)}$, or the multimodel-mean circulation change, $\overline{\delta A(w)}$. For each model, we calculate $\int_{-\infty}^{\infty} R(w)\overline{\delta A(w)}\mathrm{d}w$ – the dynamic component assuming all models have the same change in circulation – and compare this to the full dynamic component (Fig. 5a,c). We also compute $\int_{-\infty}^{\infty} \overline{R(w)}dA(w)\mathrm{d}w$ – the dynamic component assuming all models have the same cloud–circulation coupling function (Fig. 5b,d).

The intermodel spread in longwave and shortwave dynamic components is dominated by differences in circulation changes across models (Fig. 5b,d) rather than differences in cloud–circulation coupling (Fig. 5a,c). This suggests that while, as discussed in Section 3.1, a nonlinearity in $R(w)$ is an essential prerequisite for a nonzero dynamic component, and the structure of this nonlinearity and its location in vertical-velocity space affects the magnitude of the dynamic component (Fig. 3), in the case of the models analyzed here, it is the diversity in the changes in circulation which largely controls the differences in the dynamic component. In the next section we explore the aspects of the circulation changes that determine the dynamic component of the cloud feedback.

4.2 Link between dynamic component and ascent fraction

Differences in circulation changes across models drive the spread in the dynamic component. But changes in the full distribution of vertical velocity with warming are complex (Fig. 2d) and difficult to interpret in straightforward physical terms. To gain insight into how circulation impacts cloud feedbacks, we focus on a particular bulk metric of the circulation: ascent fraction, α_{up}. Ascent fraction is defined as the fraction of the model domain ascending at 500 hPa and is closely related to the subsidence fraction, which has been analyzed extensively in RCE simulations (e.g. Cronin & Wing, 2017; Wing et al., 2020; Becker & Wing, 2020; Jenney et al., 2020). We find that fractional changes in ascent fraction vary significantly between models, from -3.2–+4.9 $\%\mathrm{K}^{-1}$, with a multimodel mean value of 1.0 $\%\mathrm{K}^{-1}$. Importantly, across models, there is a strong positive correlation between fractional changes in ascent fraction and the longwave dynamic component ($r^2 = 0.71$, Fig. 6a); a strong negative correlation with the shortwave dynamic component ($r^2 = 0.75$ Fig. 6b); and a weak negative correlation with the total dynamic component ($r^2 = 0.19$, Fig. 6c). We find similar, but less robust, relationships (not shown) if we use a measure of convective aggregation [specifically the organisation index, Becker and Wing (2020)] in place of ascent fraction. The relationship between ascent fraction and longwave dynamic component is robust to the resolution of the spatial averaging (Fig. S2).

The statistical relationships between ascent fraction and the dynamic components arise from the tight coupling between changes in ascent fraction and high cloud fraction. In particular, models which tend to decrease ascent fraction under warming also tend to reduce their high cloud fraction (Fig. 7a), leading to a negative longwave dynamic component (Fig. 7b) and a positive shortwave component (Fig. 7c). The shortwave and longwave effects of high clouds approximately cancel one another (Kiehl, 1994), which offers a possible explanation as to why the net dynamic component – which is the sum of the longwave and shortwave dynamic components, both of which are linked to high cloud fraction (Fig. 7b,c) – is small (Fig. 4c). Similar relationships between high cloud fraction, ascent fraction and radiative feedbacks have also been found in GCMs in the context of narrowing of the intertropical convergence zone (Su et al., 2017). While there is a robust link between fractional changes in ascent fraction and high cloud fraction in the RCEMIP models, there are models which simultaneously have an expansion of the ascent region, and a reduction in high cloud fraction (Fig. 7a). Indeed, the response of high cloud fraction to warming is not robust across the models: There are some models in which warming leads to an expansion of high cloud fraction, though the majority have a contraction. This is also true for the wider RCEMIP archive (Wing et al., 2020). The correlations between ascent fraction, longwave and shortwave dynamic components and low cloud fraction are weaker, and not statistically significant (Fig. S3).

The relationships between ascent fraction, high cloud fraction and the dynamic components of the cloud feedback can be interpreted in simple physical terms. For example, a decrease in ascent fraction is consistent with a decrease in the area of high clouds (Fig. 7a), which in turn decreases the domain-mean shortwave cloud radiative effect and induces a negative shortwave cloud feedback (all else equal). This conceptual picture is similar to ideas explored by Pierrehumbert (1995), Lindzen et al. (2001), Mauritsen and Stevens (2015), Bony et al. (2016) and others, who argued that a decrease in high cloud cover with warming could constitute an important negative feedback on the climate system. The possibility of a reduction in ascent area and high cloud fraction with warming has been linked to the self-aggregation of convection, which is associated with a reduction of a high cloud cover and an increase in radiative cooling to space (Wing, 2019). However, it should be noted that the dynamic component of the cloud feedback captures all effects due to changes in circulation, not just those associated with self-aggregation, or indeed more generally those associated with a reduction of ascent fraction.

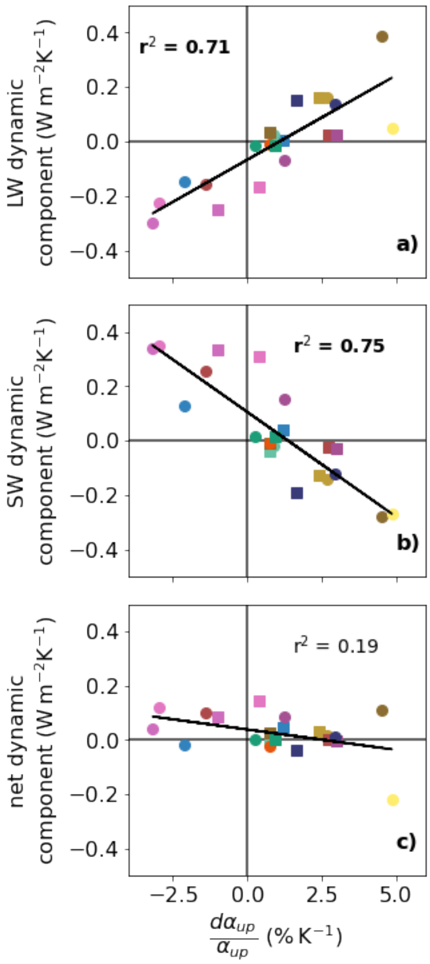

Figure 6. Fractional changes in ascent fraction between the 295 K and 300 K simulations (circles) and the 300 K and 305 K simulations (squares) versus the (a) longwave, (b) shortwave and (c) net (longwave plus shortwave) dynamic components. Colours represent different RCEMIP models, as in the legend of Fig. 4. Changes between the at 300 K and 305 K simulations for the UCLA-CRM and MESONH models are not shown as they are significant outliers (see Section 4.1). Inset text quotes the r^2 value for each panel (Pearson's correlation), with the text in bold if the correlation is statistically significant (p<0.01).

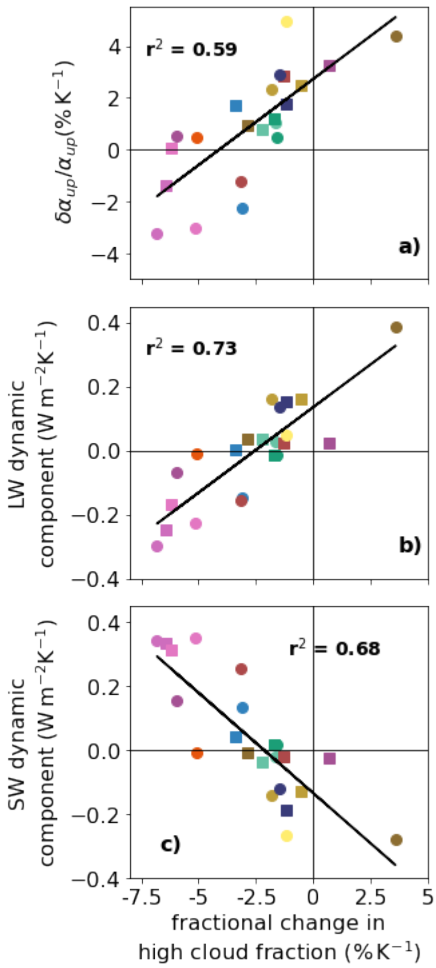

Figure 7. Fractional change in high cloud fraction with fractional changes in (a) ascent fraction, (b) longwave dynamic component and (c) shortwave dynamic component. Colors indicate different models, as in Fig. 4. UCLA-CRM and MESONH at 305-300 K have been removed from the analysis as they are significant outliers (see Section 4.1). Inset text gives the Pearson's r^2 value, with the text in bold if statistically significant (p<0.01) for the correlation between x-axis and fractional change in high cloud fraction (black). Cloud fraction is calculated at each model level following the method in Wing et al. (2020), using a threshold value of cloud condensate. We calculate the mean cloud profile for each model, and take the high cloud fraction at the peak of the profile above 500 hPa.

5 Physical processes controlling ascent fraction

The strong link between the dynamic components of the cloud feedback and ascent fraction motivates the questions: What physical processes control ascent fraction in a changing climate? And can these processes account for the spread in dynamic components across RCEMIP models? The remainder of the paper will focus on addressing these two questions.

5.1 Connecting ascent fraction to diabatic heating and static stability

To understand the processes influencing ascent fraction – and therefore the dynamic components of the cloud feedback – we first invoke the energy and mass budgets of the atmosphere. In particular, we follow the framework of Jenney et al. (2020) who derive an expression for the ascent fraction in terms of static stability and the diabatic heating rates in ascending and descending regimes. [A similar approach was taken by Byrne and Schneider (2016a, 2016b) to understand the processes controlling the width of the intertropical convergence zone]. Here we outline a version of the Jenney et al. (2020) framework in pressure coordinates, starting with the steady-state energy budgets averaged over ascending regions (denoted using the subscript "*up*") and descending regions (subscript "*dn*") separately:

$$-\omega_{up}\mathcal{S}_{up} = Q_{up} = Q^c_{up} + Q^r_{up} \tag{4}$$
$$-\omega_{dn}\mathcal{S}_{dn} = Q_{dn} = Q^c_{dn} + Q^r_{dn}, \tag{5}$$

where all quantities are means over the fraction of the domain which is either ascending (4) or descending at 500 hPa (5); ω is the vertical velocity in pressure coordinates; Q is the diabatic heating rate, consisting of radiative (Q^r) and non-radiative contributions (Q^c); and $\mathcal{S} = -(T/\theta) \times \partial\theta/\partial p$ is the static stability in pressure coordinates (T and θ represent temperature and potential temperature, respectively, and p is pressure), and all variables are evaluated at 500 hPa. Note that the "weak temperature gradient" (WTG) approximation – which suggests free-tropospheric temperature gradients in the tropics are weak owing to the small effects of planetary rotation at low latitudes (Sobel & Bretherton, 2000) – has been invoked in the derivations of (4) and (5), leading to the horizontal advection terms being dropped. The WTG approximation is expected to be applicable to the simulations being analyzed here, which have zero rotation. Indeed, in the multimodel mean, horizontal temperature advection at 500hPa is orders of magnitude smaller than vertical advection (0.0016 $\mathrm{K\,s^{-1}}$ compared to 0.24 $\mathrm{K\,s^{-1}}$), supporting the use of the WTG approximation in deriving (4) and (5). We expect that in descending regions, with little precipitation, the dominant diabatic term in the energy budget is radiative cooling. In contrast, while ascending regions also cool radiatively, latent heat release is more influential (Neelin, 1988), leading to a net positive, or warming, diabatic term (Fig. S4).

In steady state, the mass budget of the atmosphere can be expressed as:

$$\omega_{up}\alpha_{up} = -\omega_{dn}\alpha_{dn}, \tag{6}$$

where $\alpha_{dn} = 1 - \alpha_{up}$ is the fraction of the domain with descending air at 500 hPa: In simple terms, (6) states that "what goes up must come down". Combining the energy and mass budgets, an expression for the ascent fraction as a function of diabatic heating rates and static stabilities in the ascent and descent regions can be derived:

$$\alpha_{up} = \frac{1}{1 - \gamma(Q_{up}/Q_{dn})}, \tag{7}$$

where $\gamma \equiv \mathcal{S}_{dn}/\mathcal{S}_{up}$ is the ratio of the static stabilities in the descent and ascent regions. Due to the WTG approximation we expect this ratio to be approximately 1 in the free troposphere. Indeed we find that for the 295 K simulations, γ at 500 hPa ranges from 0.87–1.07 across models, with a multimodel mean of 0.97. This expression for α_{up} holds for much of the troposphere (Jenney et al., 2020) and in the following analyses we focus on the 500 hPa level.

5.2 Processes controlling ascent fraction

We have demonstrated that there exists a strong relationship between ascent fraction at 500 hPa and the dynamic components of the cloud feedback (Fig. 6). We now apply (7) to understand the processes determining ascent fraction at that level. The diabatic temperature tendency due to radiative processes, Q^r, is a standard output for the RCEMIP simulations; we compute the non-radiative diabatic temperature tendency, Q^c, as a residual from the energy budgets (4) and (5).

First, we verify that the expression (7) for α_{up} – derived using the energy and mass budgets and invoking the WTG approximation – holds at 500 hPa. We find that despite a small tendency to overestimate α_{up}, equation (7) provides a good approximation to ascent fraction across all the models (Fig. S5a). Fractional changes in simulated and approximated α_{up} between simulations, which we use in our subsequent analyses, are also very similar (Fig. S5b).

Next we linearize (7) to explore how fractional changes in ascent fraction depend on energetic processes in the atmosphere, namely diabatic heating rates and static stability:

$$\frac{\delta \alpha_{up}}{\alpha_{up}} \approx \underbrace{\frac{\gamma}{1-\gamma\frac{Q_{up}}{Q_{dn}}}\frac{Q_{up}}{Q_{dn}}}_{-\beta_1}\left[\frac{\delta Q_{up}}{Q_{up}} - \frac{\delta Q_{dn}}{Q_{dn}}\right]. \tag{8}$$

To obtain (8), we neglect fractional changes in $\gamma = \mathcal{S}_{dn}/\mathcal{S}_{up}$. This is justified again by the WTG approximation, which constrains the static stabilities in the ascent and descent regions to be similar, as discussed above. The approximation (8) broadly captures the simulated fractional changes in ascent fraction across models (Fig. S6a); accounting for changes in γ improves the approximation marginally (Fig. S6b).

Equation (8) suggests that the response of ascent fraction to warming, and therefore the dynamic components of the cloud feedback, are tightly coupled to sources of diabatic heating in the atmosphere. In particular, (8) highlights that a key control on ascent fraction is the contrast in fractional changes in diabatic heating between ascending and descending regions. If diabatic heating increases in magnitude with warming at the same fractional rate in ascending and descending regions, the ascent fraction would not change. Analogously, a larger fractional increase in diabatic heating in the ascending region relative to the descending regions implies a narrowing of ascent and *vice versa.* Note that the prefactor, $-\beta_1$, multiplying fractional changes in diabatic heating [see (8)] is a function of the climatological atmospheric state and is negative for all models analyzed.

We examine how contrasting fractional changes in diabatic heating influence changes in ascent fraction across the RCEMIP models (Fig. 8). As expected based on the approximation (8), there is a strong relationship between fractional changes in ascent fraction and the difference in fractional changes in diabatic heating between ascending and descending regions (Fig. 8a). The intermodel spread in ascent fraction changes is also linked to diabatic heating changes in the ascending region ($r^2 = 0.72$; see Fig. 8b), but there is no relationship to diabatic heating changes in the descending region ($r^2 = 0.01$).

The relationship between ascent fraction and diabatic heating can be interpreted in the following way: An increase in SST leads to a positive fractional change in Q_{dn} (i.e.

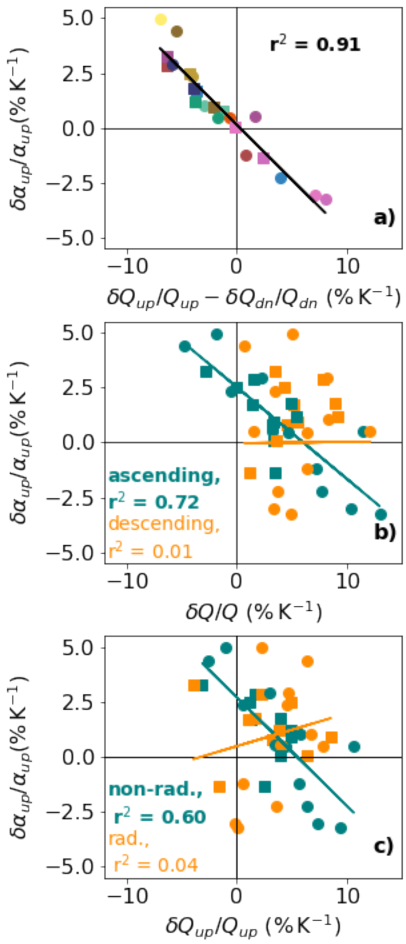

Figure 8. Relationships between fractional changes in ascent fraction and (a) $\delta Q_{up}/Q_{up}$ - $\delta Q_{dn}/Q_{dn}$; (b) fractional changes in ascent region diabatic heating rate ($\delta Q_{up}/Q_{up}$, teal) and descent region diabatic heating rate ($\delta Q_{dn}/Q_{dn}$, orange); and (c) as in (b), but for ascent region radiative (δQ^r_{up} $/Q^r_{up}$) and non-radiative ($\delta Q^c_{up}/Q^c_{up}$) diabatic heating rates. Colors in (a) indicate different models, as in Fig. 4. Changes for the UCLA-CRM and MESONH models between the 300 K and 305 K simulations have been removed from the analysis as they are significant outliers (see Section 4.1). Inset text quotes the Pearson's r^2 values, with the text in bold if the correlation is statistically significant (p<0.01).

Q_{dn} becomes more negative) in all models (Fig. 8b), consistent with increased radiative cooling from a warmer, moister atmosphere (Pendergrass & Hartmann, 2014). This effect, all else being equal, would drive an increase in ascent fraction according to (8). However, changes in Q_{up} with SST are less consistent across models: while the majority of pairs of model simulations (18 of the 22) have a positive fractional change in Q_{up}, corresponding to a decrease in α_{up} should no other changes occur, a minority of simulation pairs show a fractional decrease in Q_{up}. The relative sizes of fractional changes in Q_{up} and Q_{dn} determine the change in α_{up}, and only six of the simulation pairs have a sufficiently positive fractional change in Q_{up} to overcome the change in Q_{dn} (Fig. 8a). Therefore, while relative changes in Q_{up} versus Q_{dn} determine changes in α_{up}, the spread between models of fractional changes in α_{up}, and therefore the dynamic component of the cloud feedback, are largely due to variations between models in the response of Q_{up}.

5.3 Radiative versus non-radiative diabatic heating

To further probe the processes driving intermodel spread in ascent fraction changes, we divide the total diabatic heating in ascent regions into radiative and non-radiative components (i.e. $Q_{up} = Q^r_{up} + Q^c_{up}$):

$$\frac{\delta Q_{up}}{Q_{up}} = \underbrace{\frac{Q^c_{up}}{Q^c_{up} + Q^r_{up}}}_{\beta_2} \frac{\delta Q^c_{up}}{Q^c_{up}} - \underbrace{- \frac{Q^r_{up}}{Q^c_{up} + Q^r_{up}}}_{\beta_3} \frac{\delta Q^r_{up}}{Q^r_{up}}, \tag{9}$$

where both β_2 and β_3 are both positive as Q^c_{up} (largely driven by latent heating, a positive term) is positive, Q^r_{up} is negative (from radiative cooling) and $|Q^c_{up}| > |Q^r_{up}|$ (Fig. S4b). Substituting (9) into (8) leads to:

$$\frac{\delta \alpha_{up}}{\alpha_{up}} = -\beta_1 \left[\beta_2 \frac{\delta Q^c_{up}}{Q^c_{up}} - \beta_3 \frac{\delta Q^r_{up}}{Q^r_{up}} - \frac{\delta Q_{dn}}{Q_{dn}} \right]. \tag{10}$$

Equation (10) again broadly captures variations in the fractional change in ascent fraction (Fig. S6c) and highlights how both radiative and non-radiative diabatic heating in ascending regions influence ascent fraction, though the relative importance of each term is unclear. We find a statistically significant correlation between fractional changes in non-radiative diabatic heating and fractional changes in ascent fraction ($r^2 = 0.60$; Fig. 8c), but no significant correlation with radiative heating changes ($r^2 = 0.04$). This suggests that it is the non-radiative diabatic heating response to warming in the ascent region which is most strongly linked to ascent fraction.

To what extent can a similar argument be made to explain the differing roles of circulation changes in cloud feedbacks across models? Fractional changes in the diabatic heating contrast between ascending and descending regions correlate significantly with the spread in longwave dynamic component ($r^2 = 0.61$, not shown). The dynamic component is negatively correlated with these terms: If fractional changes in Q_{up} increase relative to fractional changes in Q_{dn}, ascent fraction decreases and the longwave component of the cloud feedback is negative.

The next logical question, following the analysis above, is which non-radiative processes may be contributing to the spread in Q^c_{up} and thus to differing ascent fraction responses. Non-radiative diabatic heating is composed of contributions from latent heating, detrainment and dry static energy transport due to turbulence (Jenney et al., 2020). We do not isolate the roles of these individual non-radiative diabatic heating processes here, given the required data are not available in the RCEMIP archive, but this would be an interesting avenue for future research. Another interesting question is whether intermodel differences in how non-radiative heating changes with warming arise from differing convective parameterizations, differing cloud physics, surface fluxes or other factors. Schiro et al. (2019) explore this question by perturbing convective and cloud parameterizations in a GCM to recreate the spread in ascent fraction change across the CMIP5 ensemble, and find that convective parameterizations are key to explaining differing ascent-fraction responses.

6 Discussion

Cloud feedbacks remain one of the largest sources of uncertainty in climate projections. While the role of circulation changes in modulating large-scale cloud feedbacks is limited in global climate models (Byrne & Schneider, 2018), the influence of circulation on cloud responses in high-resolution models and in the real Earth system is an open question.

Here we investigate cloud–circulation coupling using idealized cloud-resolving simulations in radiative-convective equilibrium (Wing et al., 2018, 2020). Cloud feedbacks are decomposed into dynamic and thermodynamic components following Bony et al. (2004) in order to directly quantify the role of circulation changes (i.e. the dynamic component). In contrast to the negligible dynamic components in global models found in previous studies, we find a wide range of dynamic components across the RCEMIP models, some of which contribute substantially to the total cloud feedback. Some models have a strong positive longwave dynamic component, some have a strong negative longwave dynamic component, and some have a small dynamic component. In general, the shortwave dynamic component for a given model is of similar magnitude and opposite sign to the longwave dynamic component.

We establish a strong link between the dynamic component of the cloud feedback and the degree to which the ascent region narrows or widens with warming. Models which have the strongest narrowing of ascent with warming also have the strongest longwave and shortwave dynamic components of the cloud feedback, due to decreases in high cloud fraction. The dynamic components and changes in ascent fraction are linked – via the energy and mass budgets of the atmosphere – to diabatic heating rates in ascending and descending regions. Specifically, intermodel differences in how ascent fraction changes with warming are coupled to differences in non-radiative diabatic processes, including latent heating, in ascending regions. However, a stronger predictor of ascent region narrowing or expansion – and therefore a strong predictor of the dynamic component – is the contrast in diabatic heating changes between ascending and descending regions.

Our study highlights a number of interesting possibilities for further research. First, a key question is the degree to which different non-radiative diabatic processes – including latent heat release, convective entrainment and cloud microphysics – drive the response of ascent fraction and high-cloud fraction to warming. Also, what is the effect of a large-scale circulation, for example driven by SST gradients, on the relationships between cloud feedbacks and circulation examined here? And finally, does the substantial influence of circulation on clouds found in tropical high-resolution models have implications for estimates of cloud feedbacks and climate sensitivity in global models? Pursuing these questions, perhaps through analyses of observations and a hierarchy of models, will further build understanding of the role of cloud–circulation coupling in the climate system.

543 # Appendix A

Table A1. The RCEMIP models analyzed in this study. For more details about individual models see Wing et al. (2020).

Full Name	Abbreviation
Cloud Model 1, cm1r19.6	CM1
Das Atmosphaerische Modell	dam
ICOsahedral Nonhydrostatic-2.3.00, LEM config.	ICON_LEM_CRM
ICOsahedral Nonhydrostatic-2.3.00, NWP config.	ICON_NWP_CRM
Meso-NH v5.4.1	MESONH
System for Atmospheric Modeling 6.11.2	SAM_CRM
SCALE v5.2.5	SCALE
UCLA Large-Eddy Simulation model	UCLA_CRM
UK Met Office Idealized Model v11.0 - CASIM	UKMOi-vn11.0-CASIM
UK Met Office Idealized Model v11.0 - RA1-T	UKMOi-vn11.0-RA1-T
UK Met Office Idealized Model v11.0 - RA1-T	UKMOi-vn11.0-RA1-T-nocloud
Weather Research and Forecasting model v3.5.1	WRF_COL_CRM

Acknowledgments

We acknowledge funding from the UK Natural Environment Research Council (Grant NE/T006269/1) and the European Union's Horizon 2020 Research and Innovation Program under Marie Skłodowska-Curie Grant Agreement 794063. We thank the German Climate Computing Center (DKRZ) for hosting the standardized RCEMIP data, which is publicly available at `http://hdl.handle.net/21.14101/d4beee8e-6996-453e-bbd1-ff53b6874c0e`. We further thank Peter Hill, Chris Holloway, Hugo Lambert, Monisha Natchair, Levi Silvers, Mark Webb and Allison Wing for helpful discussions and suggestions.

References

Bao, J., Sherwood, S. C., Colin, M., & Dixit, V. (2017). The robust relationship between extreme precipitation and convective organization in idealized numerical modeling simulations. *Journal of Advances in Modeling Earth Systems*, *9*(6), 2291–2303. doi: 10.1002/2017MS001125

Becker, T., & Wing, A. A. (2020). Understanding the extreme spread in climate sensitivity within the radiative-convective equilibrium model intercomparison project. *Journal of Advances in Modeling Earth Systems*, *12*(10), e2020MS002165. doi: 10.1029/2020MS002165

Bony, S., Colman, R., Kattsov, V. M., Allan, R. P., Bretherton, C. S., Dufresne, J., ... Webb, M. J. (2006). How well do we understand and evaluate climate change feedback processes? *Journal of Climate*, *19*(15), 3445–3482. doi: 10.1175/JCLI3819.1

Bony, S., Dufresne, J.-L., Le Treut, H., Morcrette, J.-J., & Senior, C. (2004). On dynamic and thermodynamic components of cloud changes. *Climate Dynamics*, *22*(2), 71–86. doi: 10.1007/s00382-003-0369-6

Bony, S., Stevens, B., Coppin, D., Becker, T., Reed, K. A., Voigt, A., & Medeiros, B. (2016). Thermodynamic control of anvil cloud amount. *Proceedings of the National Academy of Sciences*, *113*(32), 8927–8932. doi: 10.1073/pnas.1601472113

Bony, S., Stevens, B., Frierson, D. M. W., Jakob, C., Kageyama, M., Pincus, R., ... Webb, M. J. (2015). Clouds, circulation and climate sensitivity. *Nature Geoscience*, *8*(4), 261–268. doi: 10.1038/ngeo2398

Bretherton, C. S., Blossey, P. N., & Khairoutdinov, M. (2005). An energy-balance analysis of deep convective self-aggregation above uniform SST. *Journal of the Atmospheric Sciences*, *62*(12), 4273–4292. doi: 10.1175/JAS3614.1

Byrne, M. P., & Schneider, T. (2016a). Energetic constraints on the width of the intertropical convergence zone. *Journal of Climate*, *29*, 4709–4721. doi: 10.1175/JCLI-D-15-0767.1

Byrne, M. P., & Schneider, T. (2016b). Narrowing of the ITCZ in a warming climate: Physical mechanisms. *Geophysical Research Letters*, *43*, 11,350–11,357.

Byrne, M. P., & Schneider, T. (2018). Atmospheric dynamics feedback: Concept, simulations, and climate implications. *Journal of Climate*, *31*(8), 3249–3264. doi: 10.1175/JCLI-D-17-0470.1

Ceppi, P., Brient, F., Zelinka, M. D., & Hartmann, D. L. (2017). Cloud feedback mechanisms and their representation in global climate models. *WIREs Climate Change*, *8*(4), e465. doi: 10.1002/wcc.465

Cess, R. D., & Potter, G. L. (1988). A methodology for understanding and intercomparing atmospheric climate feedback processes in general circulation models. *Journal of Geophysical Research: Atmospheres*, *93*(D7), 8305–8314. doi: 10.1029/JD093iD07p08305

Coppin, D., & Bony, S. (2018). On the interplay between convective aggregation, surface temperature gradients, and climate sensitivity. *Journal of Advances in Modeling Earth Systems*, *10*(12), 3123–3138. doi: 10.1029/2018MS001406

Cronin, T. W., & Wing, A. A. (2017). Clouds, circulation, and climate sensitivity in a radiative-convective equilibrium channel model. *Journal of Advances in Modeling Earth Systems*, *9*(8), 2883–2905. doi: 10.1002/2017MS001111

Hartmann, D. L., & Larson, K. (2002). An important constraint on tropical cloud - climate feedback. *Geophysical Research Letters*, *29*(20), 12-1-12-4. doi: 10.1029/2002GL015835

Hartmann, D. L., Moy, L. A., & Fu, Q. (2001). Tropical convection and the energy balance at the top of the atmosphere. *Journal of Climate*, *14*(24), 4495–4511. doi: 10.1175/1520-0442(2001)014⟨4495:TCATEB⟩2.0.CO;2

Held, I. M., Hemler, R. S., & Ramaswamy, V. (1993). Radiative-convective equilibrium with explicit two-dimensional moist convection. *Journal of Atmo-*

spheric Sciences, *50*(23), 3909–3927. doi: 10.1175/1520-0469(1993)050⟨3909:RCEWET⟩2.0.CO;2

Holloway, C. E., & Woolnough, S. J. (2016). The sensitivity of convective aggregation to diabatic processes in idealized radiative-convective equilibrium simulations. *Journal of Advances in Modeling Earth Systems*, *8*(1), 166-195. doi: 10.1002/2015MS000511

Jenney, A. M., Randall, D. A., & Branson, M. D. (2020). Understanding the response of tropical ascent to warming using an energy balance framework. *Journal of Advances in Modeling Earth Systems*, *12*(6), e2020MS002056. doi: 10.1029/2020MS002056

Kiehl, J. (1994). On the observed near cancellation between longwave and shortwave cloud forcing in tropical regions. *Journal of Climate*, 559–565. doi: 10.1175/1520-0442(1994)007⟨0559:OTONCB⟩2.0.CO;2

Lindzen, R. S., Chou, M.-D., & Hou, A. Y. (2001). Does the earth have an adaptive infrared iris? *Bulletin of the American Meteorological Society*, *82*(3), 417-432. doi: 10.1175/1520-0477(2001)082⟨0417:DTEHAA⟩2.3.CO;2

Lutsko, N. J. (2018). The relationship between cloud radiative effect and surface temperature variability at El Niño-Southern Oscillation frequencies in CMIP5 models. *Geophysical Research Letters*, *45*(19), 10,599–10,608. doi: 10.1029/2018GL079236

Mauritsen, T., & Stevens, B. (2015). Missing iris effect as a possible cause of muted hydrological change and high climate sensitivity in models. *Nature Geoscience*, *8*(5), 346–351. doi: 10.1038/ngeo2414

Muller, C. J., & Held, I. M. (2012). Detailed investigation of the self-aggregation of convection in cloud-resolving simulations. *Journal of the Atmospheric Sciences*, *69*(8), 2551–2565. doi: 10.1175/JAS-D-11-0257.1

Neelin, J. D. (1988). A simple model for surface stress and low-level flow in the tropical atmosphere driven by prescribed heating. *Quarterly Journal of the Royal Meteorological Society*, *114*(481), 747–770. doi: 10.1175/2008JCLI2303.1

Pendergrass, A. G., & Hartmann, D. L. (2014). The atmospheric energy constraint on global-mean precipitation change. *Journal of Climate*, *27*(2), 757-768. doi: 10.1175/JCLI-D-13-00163.1

Pendergrass, A. G., Reed, K. A., & Medeiros, B. (2016). The link between extreme precipitation and convective organization in a warming climate: Global radiative-convective equilibrium simulations. *Geophysical Research Letters*, *43*(21), 11,445-11,452. doi: 10.1002/2016GL071285

Pierrehumbert, R. T. (1995, 05). Thermostats, radiator fins, and the local runaway greenhouse. *Journal of the Atmospheric Sciences*, *52*(10), 1784–1806. doi: 10.1175/1520-0469(1995)052⟨1784:TRFATL⟩2.0.CO;2

Romps, D. M. (2020). Climate sensitivity and the direct effect of carbon dioxide in a limited-area cloud-resolving model. *Journal of Climate*, *33*(9), 3413–3429. doi: 10.1175/JCLI-D-19-0682.1

Romps, D. M., & Kuang, Z. (2011). A transilient matrix for moist convection. *Journal of the Atmospheric Sciences*, *68*(9), 2009–2025. doi: 10.1175/2011JAS3712.1

Schiro, K. A., Su, H., Wang, Y., Langenbrunner, B., Jiang, J. H., & Neelin, J. D. (2019). Relationships between tropical ascent and high cloud fraction changes with warming revealed by perturbation physics experiments in CAM5. *Geophysical Research Letters*, *46*(16), 10112-10121. doi: 10.1029/2019GL083026

Sherwood, S. C., Bony, S., & Dufresne, J.-L. (2014). Spread in model climate sensitivity traced to atmospheric convective mixing. *Nature*, *505*, 37–42. doi: {10.1038/nature12829}

Sherwood, S. C., Webb, M. J., Annan, J. D., Armour, K. C., Forster, P. M., Hargreaves, J. C., . . . Zelinka, M. D. (2020). An assessment of Earth's climate sensitivity using multiple lines of evidence. *Reviews of Geophysics*, *58*(4), e2019RG000678. doi: 10.1029/2019RG000678

Silvers, L. G., Reed, K. A., & Wing, A. A. (submitted). The response of the large-scale tropical circulation to warming. *Journal of Advances in Modeling Earth Systems*.

Singh, M. S., & O'Gorman, P. A. (2015). Increases in moist-convective updraught velocities with warming in radiative-convective equilibrium. *Quarterly Journal of the Royal Meteorological Society*, *141*(692), 2828-2838. doi: https://doi.org/10.1002/qj.2567

Sobel, A. H., & Bretherton, C. S. (2000). Modeling tropical precipitation in a single column. *J. Climate*, *13*, 4378-4392. doi: 10.1175/1520-0442(2000)013⟨4378:MTPIAS⟩2.0.CO;2

Su, H., Jiang, J. H., Neelin, J. D., Shen, T. J., Zhai, C., Yue, Q., ... Yung, Y. L. (2017). Tightening of tropical ascent and high clouds key to precipitation change in a warmer climate. *Nature Communications*, *8*. doi: 10.1038/ncomms15771

Webb, M. J., Andrews, T., Bodas-Salcedo, A., Bony, S., Bretherton, C. S., Chadwick, R., ... Watanabe, M. (2017). The cloud feedback model intercomparison project (CFMIP) contribution to CMIP6. *Geoscientific Model Development*, *10*(1), 359–384. doi: 10.5194/gmd-10-359-2017

Wing, A. A. (2019). Self-aggregation of deep convection and its implications for climate. *Current Climate Change Reports*, *5*(1), 1-11. doi: 10.1007/s40641-019-00120-3

Wing, A. A., & Cronin, T. W. (2016a). Self-aggregation of convection in long channel geometry. *Quarterly Journal of the Royal Meteorological Society*, *142*(694), 1–15. doi: 10.1002/qj.2628

Wing, A. A., & Cronin, T. W. (2016b). Self-aggregation of convection in long channel geometry. *Quarterly Journal of the Royal Meteorological Society*, *142*(694), 1-15. doi: h10.1002/qj.2628

Wing, A. A., Emanuel, K., Holloway, C. E., & Muller, C. (2017). Convective self-aggregation in numerical simulations: A review. In R. Pincus, D. Winker, S. Bony, & B. Stevens (Eds.), *Shallow Clouds, Water Vapor, Circulation, and Climate Sensitivity* (pp. 1–25). Springer International Publishing. doi: 10.1007/978-3-319-77273-8_1

Wing, A. A., & Emanuel, K. A. (2014). Physical mechanisms controlling self-aggregation of convection in idealized numerical modeling simulations. *Journal of Advances in Modeling Earth Systems*, *6*(1), 59–74. doi: 0.1002/2013MS000269

Wing, A. A., Reed, K. A., Satoh, M., Stevens, B., Bony, S., & Ohno, T. (2018). Radiative–convective equilibrium model intercomparison project. *Geoscientific Model Development*, *11*(2), 793–813. doi: 10.5194/gmd-11-793-2018

Wing, A. A., Stauffer, C. L., Becker, T., Reed, K. A., Ahn, M.-S., Arnold, N. P., ... Zhao, M. (2020). Clouds and convective self-aggregation in a multimodel ensemble of radiative-convective equilibrium simulations. *Journal of Advances in Modeling Earth Systems*, *12*(9), e2020MS002138. doi: 10.1029/2020MS002138

Wyant, M. C., Bretherton, C. S., Bacmeister, J. T., Kiehl, J. T., Held, I. M., Zhao, M., ... Soden, B. J. (2006). A comparison of low-latitude cloud properties and their response to climate change in three AGCMs sorted into regimes using mid-tropospheric vertical velocity. *Climate Dynamics*, *27*, 261-279. doi: 10.1007/s00382-006-0138-4

Wyant, M. C., Khairoutdinov, M., & Bretherton, C. S. (2006). Climate sensitivity and cloud response of a GCM with a superparameterization. *Geophysical Research Letters*, *33*(6). doi: 10.1029/2005GL025464

Zelinka, M. D., & Hartmann, D. L. (2010). Why is longwave cloud feedback positive? *Journal of Geophysical Research: Atmospheres*, *115*(D16). doi: 0.1029/2010JD013817

Zelinka, M. D., Myers, T. A., McCoy, D. T., Po-Chedley, S., Caldwell, P. M., Ceppi, P., ... Taylor, K. E. (2020). Causes of higher climate sensitivity in CMIP6 models. *Geophysical Research Letters*. doi: 10.1029/2019GL085782

Supporting Information for "Effects of circulation on tropical cloud feedbacks in high-resolution simulations"

Anna Mackie[1], Michael P. Byrne[1,2]

[1]School of Earth and Environmental Sciences, University of St Andrews

[2]Atmospheric, Oceanic and Planetary Physics, University of Oxford

Contents of this file

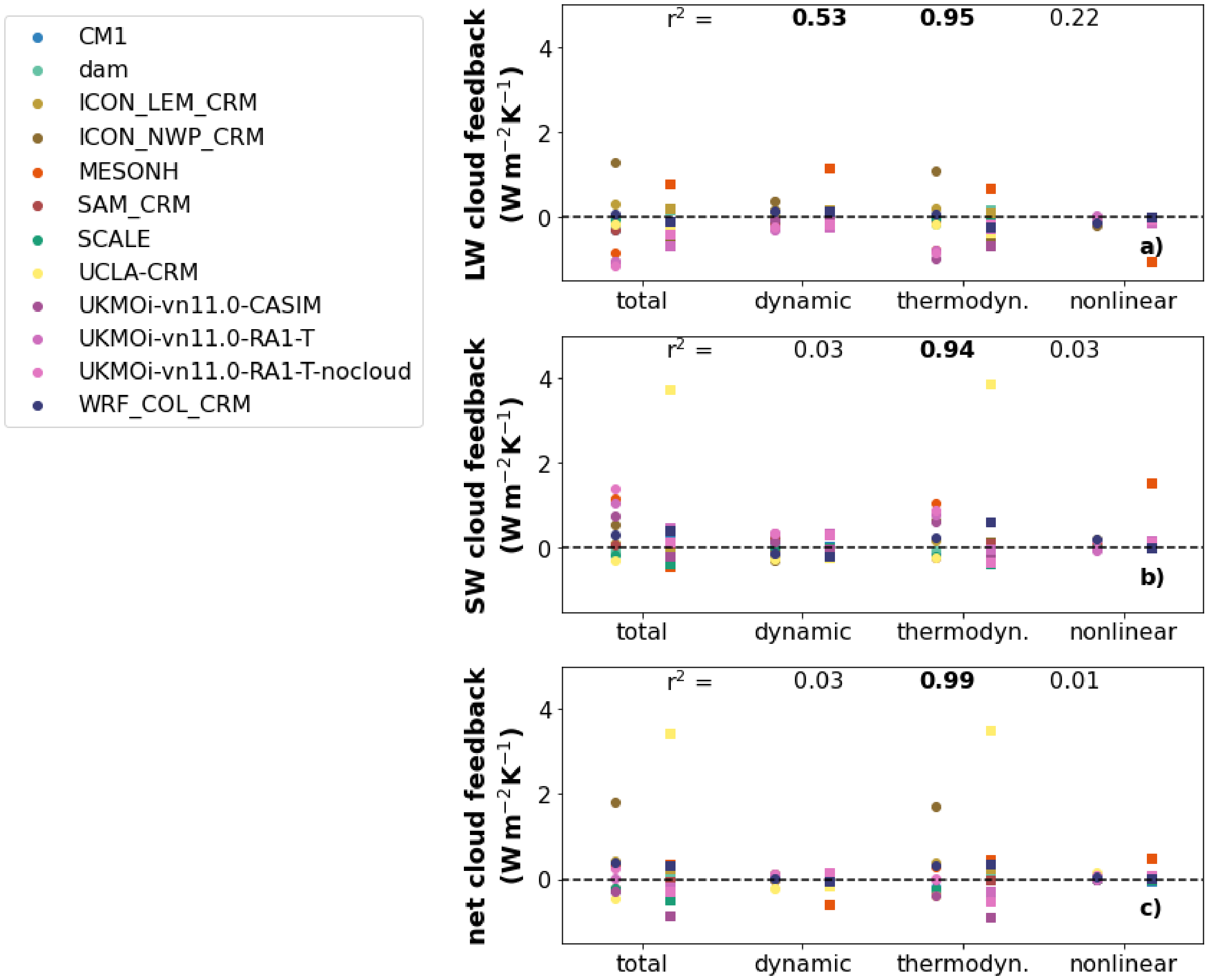

Figure S1. Similar to Figure 4, but without the outlier points removed. Two sets of feedbacks are computed: between the 295 K and 300 K simulations (circles) and between the 300 K and 305 K simulations (squares). Colours indicate different models, as in legend of Fig. 4. The identified anomalous feedbacks are for the UCLA-CRM model (computed between the 300 K and 300 K simulations, yellow squares), which has an anomalously large shortwave thermodynamic component, and the MESONH model (also computed between the 300 K and 300 K simulations, red squares), which has anomalously large thermodynamic, dynamic and nonlinear components. Inset text in this and subsequent figures gives the Pearson's r^2 value, with the text in bold if statistically significant (p<0.01).

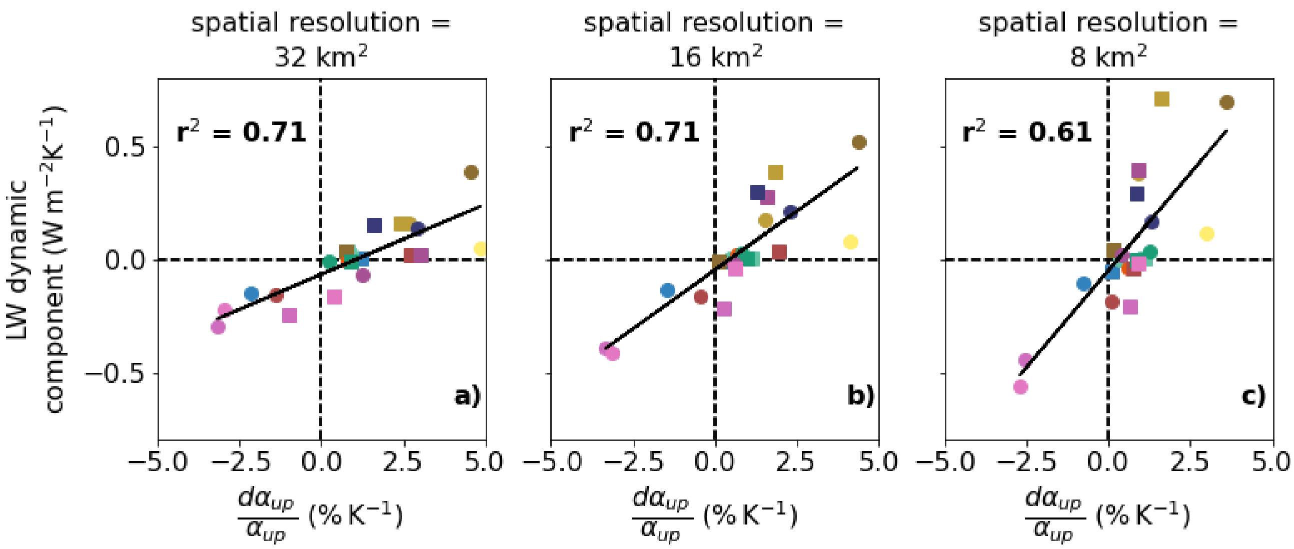

Figure S2. Testing the sensitivity of Figure 6a [reproduced here for comparison as panel (a)] to the resolution of spatial averaging. Dynamic components computed for the 300 K minus 295 K simulations (circles) and the 305 K minus 300 K simulations (squares). Colours indicate different models, as in legend of Figure S1.

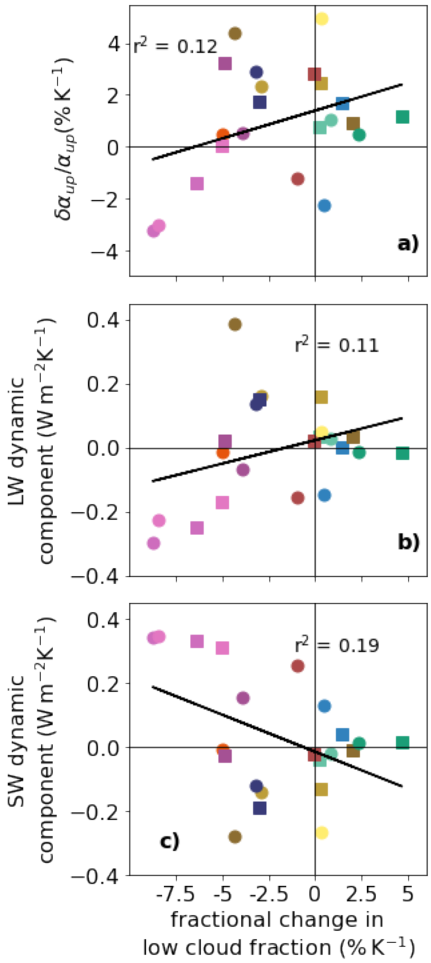

Figure S3. As in Figure 6 but here for low-cloud fraction.

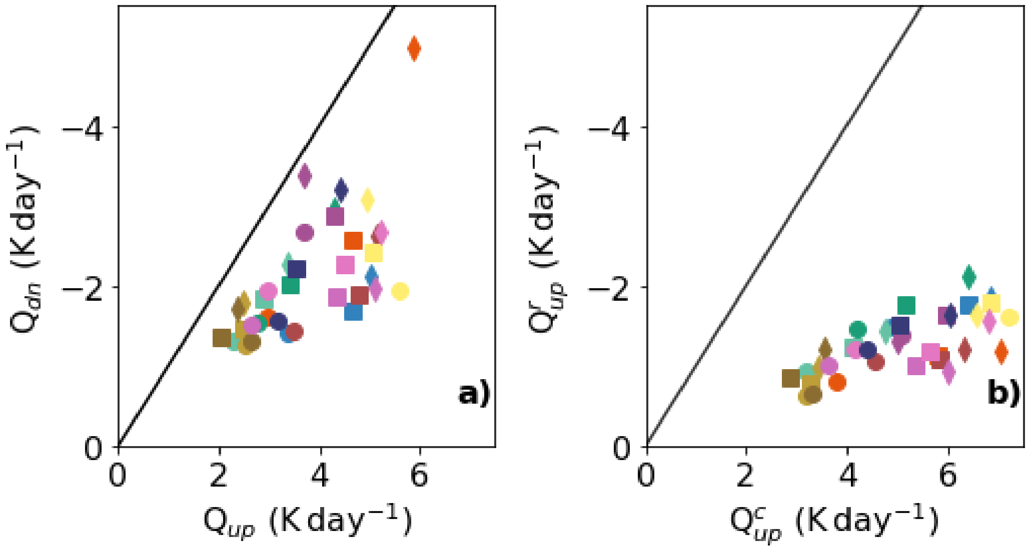

Figure S4. (a) Model values of Q_{up} against Q_{dn}, circles, sqaure and triangles indicate the 295 K, 300 K and 305 K simulations, respectively. Black lines show where $|Q_{dn}| = |Q_{up}|$ to aid comparison of magnitudes. Panel (b), as for panel (a), but for Q^r_{up} versus Q^c_{up}

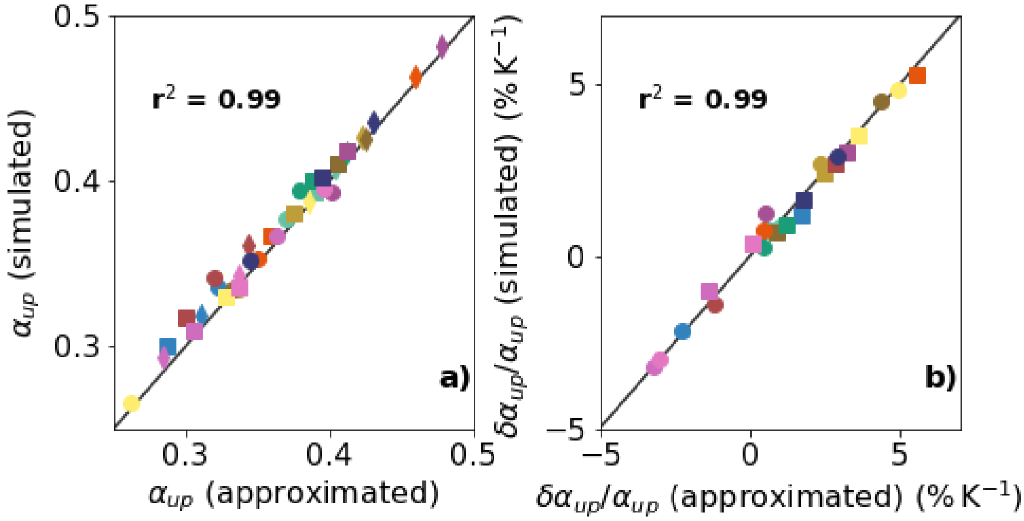

Figure S5. (a) Ascent fraction α_{up} as approximated by (7) (Jenney et al., 2020) versus simulated ascent fraction. Symbols represent different temperatures: circles indicate the 295 K simulations, squares the 300 K simulations, and triangles the 305 K simulations. (b) Fractional changes in approximated versus simulated α_{up}, circles indicate 300 K minus 295 K, squares indicate 305 K minus 300 K. UCLA-CRM and MESONH at 305-300 K have been removed from the analysis as they are significant outliers (Fig. S1).

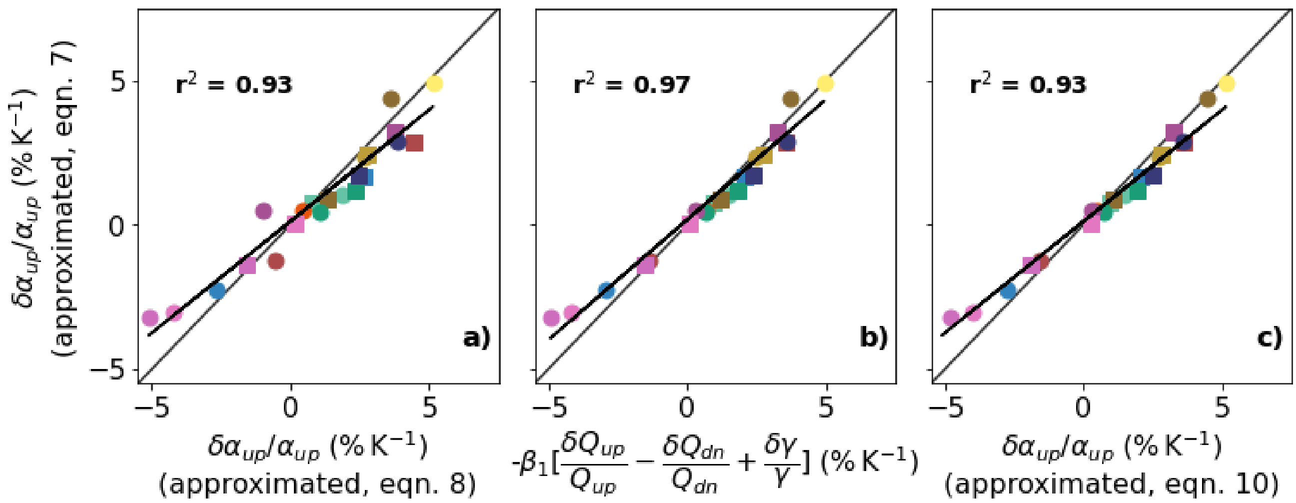

Figure S6. (a) Approximation of the fractional change in ascent fraction by (8) versus that computed from (7) and calculating the fractional changes. The 1:1 line is marked, as is the regression line from the approximation, which has a slope of 0.77. (b) As for panel (a) but the x-axis values are calculated including fractional changes in γ; the slope of this regression line is 0.83. (c) As for panel (a) but the x-axis values are calculated using (10); the slope of this regression line is 0.77. UCLA-CRM and MESONH at 305-300 K have been removed from the analysis as they are significant outliers (Fig. S1).

References

Jenney, A. M., Randall, D. A., & Branson, M. D. (2020). Understanding the response of tropical ascent to warming using an energy balance framework. *Journal of Advances in Modeling Earth Systems*, *12*(6), e2020MS002056. doi: 10.1029/2020MS002056